AD-A062 162 RUTGERS - THE STATE UNIV PISCATAWAY NJ DEPT OF MECHA--ETC F/G 11/6
X-RAY DOUBLE-CRYSTAL DIFFRACTOMETER DETERMINATION OF EXCESS DIS--ETC(U)
DEC 78 S WEISSMANN, R YAZICI, T TSAKALAKOS N00014-77-C-0191

UNCLASSIFIED NL

1 OF 1
AD
A062162

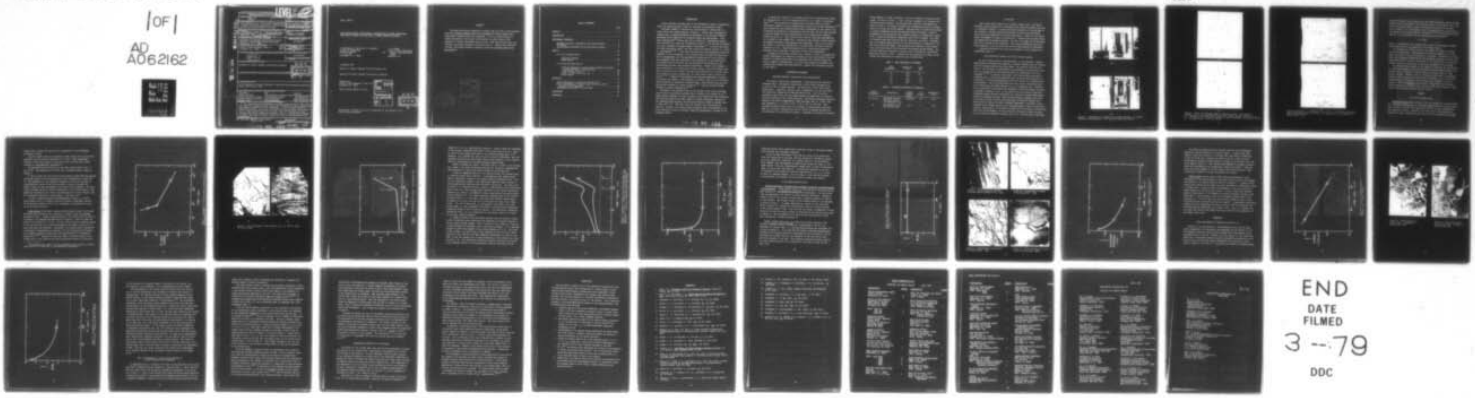

END
DATE
FILMED
3-79
DDC

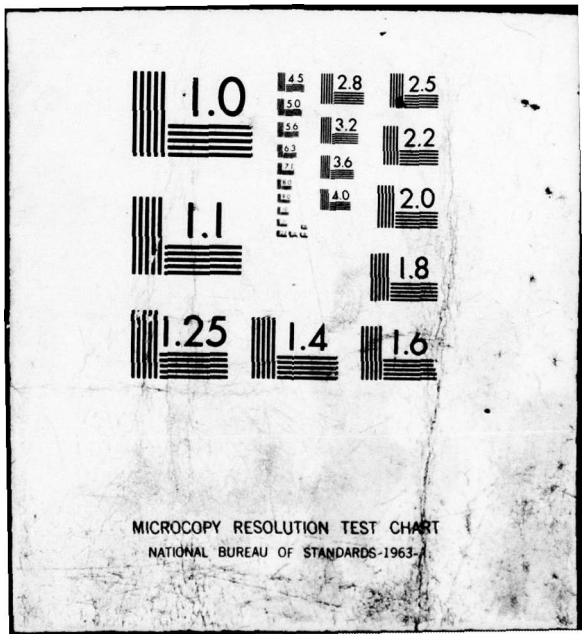
1.0
1.1
1.25
1.4
1.6
1.8
2.0
2.2
2.5
2.8
3.2
3.6
4.0
4.5
5.0
5.6
6.3
MICROCOPY RESOLUTION TEST CHART
NATIONAL BUREAU OF STANDARDS-1963-A

SECURITY CLASSIFICATION OF THIS PAGE (When Data Entered)

LEVEL II

REPORT DOCUMENTATION PAGE

READ INSTRUCTIONS BEFORE COMPLETING FORM

1. REPORT NUMBER	2. GOVT ACCESSION NO.	3. RECIPIENT'S CATALOG NUMBER
ONR-R-1		

4. TITLE (and Subtitle)
X-Ray Double-Crystal Diffractometer Determination of Excess Dislocation Densities of Surface Layer and Bulk in Stress Corrosion Cracking.

5. TYPE OF REPORT & PERIOD COVERED
Interim Technical Report. 1 Feb 1977-30 Nov. 1978.

6. PERFORMING ORG. REPORT NUMBER

7. AUTHOR(s)
S. Weissmann, R. Yazici, T. Tsakalakos, Rutgers University, and I. R. Kramer, David W. Taylor Naval Ship R & D Center, Annapolis, Md.

8. CONTRACT OR GRANT NUMBER(s)
N00014-77-C-0191

9. PERFORMING ORGANIZATION NAME AND ADDRESS
Department of Mechanics and Materials Science, College of Engineering, Rutgers University, Piscataway, N. J. 08854

10. PROGRAM ELEMENT, PROJECT, TASK AREA & WORK UNIT NUMBERS
NR 036-119

11. CONTROLLING OFFICE NAME AND ADDRESS
Office of Naval Research (Code 471)
Arlington, Va. 22217

12. REPORT DATE
December, 1978

13. NUMBER OF PAGES
32

14. MONITORING AGENCY NAME & ADDRESS *(if different from Controlling Office)*
38 p.

15. SECURITY CLASS. *(of this report)*
Unclassified

15a. DECLASSIFICATION/DOWNGRADING SCHEDULE

16. DISTRIBUTION STATEMENT *(of this Report)*
Approved for public release; distribution unlimited

DDC RECEIVED DEC 14 1978 D

17. DISTRIBUTION STATEMENT *(of the abstract entered in Block 20, if different from Report)*

18. SUPPLEMENTARY NOTES
To be presented at Spring Conference of American Crystallographic Association, Hawaii, March 26-30, 1979

19. KEY WORDS *(Continue on reverse side if necessary and identify by block number)*

Experiment	Bulk	Fracture
Stress Corrosion	304 Austenitic Stainless Steel	X-Ray Double-Crystal
Stress Corrosion Cracking	Alpha-Titanium Alloys	Diffractometry
Excess Dislocation Density	Crack Nucleation	X-Ray Rocking Curves
Surface Layer	Crack Propagation	X-Ray Topography

20. ABSTRACT *(Continue on reverse side if necessary and identify by block number)*

The excess dislocation densities in surface layer and bulk of 304 stainless steel and titanium aluminum alloys were determined by X-ray rocking curve measurements combined with X-ray topography. Up to a critical density of excess dislocations, the surface layer exerted a barrier effect on the egression of excess dislocations from the bulk. When this critical value was exceeded, macroscopic mechanical instability set in. Methods were presented to predict the stress corrosion lifetime of alloys by non-destructive X-ray measurements.

DD FORM 1 JAN 73 1473 EDITION OF 1 NOV 65 IS OBSOLETE S/N 0102-LF-014-6601

UNCLASSIFIED

SECURITY CLASSIFICATION OF THIS PAGE (When Data Entered)

AD A062162

DDC FILE COPY

78 12 04 132 410 971

Report ONR-R-1

X-RAY DOUBLE-CRYSTAL DIFFRACTOMETER DETERMINATION OF EXCESS DISLOCATION DENSITIES OF SURFACE LAYER AND BULK IN STRESS CORROSION CRACKING

S. Weissmann, R. Yazici and T. Tsakalakos
College of Engineering
Rutgers University
P. O. Box 909
Piscataway, N. J. 08854

and

I. R. Kramer
David W. Taylor Naval Ship
Research and Development
Center
Annapolis, Md

1 December 1978

Report for Period 1 February 1977-30 November 1978

Approved for public release; distribution unlimited

Prepared for
Office of Naval Research (Code 471)
Arlington, VA 22217

Under Contract N00014-77-C-0191

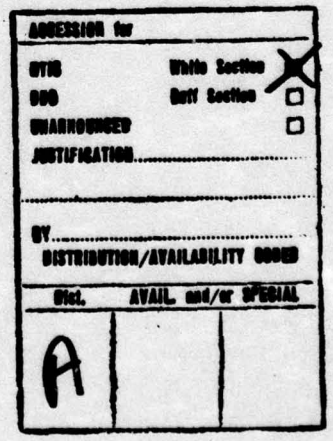

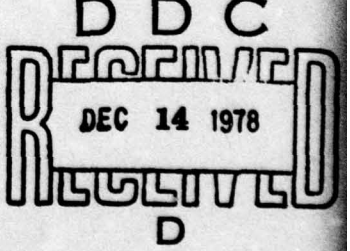

ABSTRACT

The excess dislocation densities in surface layer and bulk of 304 stainless steel and titanium aluminum alloys were determined by X-ray rocking curve measurements combined with X-ray topography. Up to a critical density of excess dislocations, the surface layer exerted a barrier effect on the egression of excess dislocations from the bulk. When this critical value was exceeded, macroscopic mechanical instability set in. Methods were presented to predict the stress corrosion lifetime of alloys by non-destructive X-ray measurements.

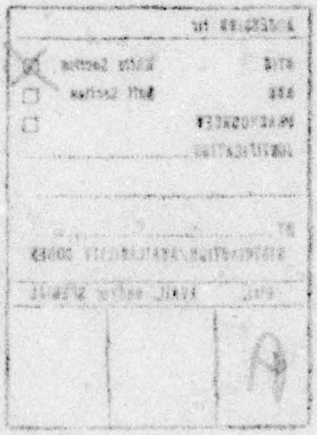

TABLE OF CONTENTS

INTRODUCTION

Stress corrosion cracking (SCC) is the phenomenon of metal disintegration under the combined action of chemical corrosion and mechanical stress.

Although a number of theories have been proposed to explain SCC, no single theory has received general acceptance. Indeed, some investigators[1] maintain that no general mechanism is applicable to SCC and that different mechanisms may be operative for different metals and environments. Thus, some investigators[2-4] believe that SCC is caused by a preferential dissolution process at the crack tip ("dissolution theory"). SCC has been attributed, also, to a decrease of surface energy by absorption.[5-7] A brittle film model was first proposed by Logan,[8] and this concept was pursued further by a number of investigators.[9,10] It was first held that the crack propagation rates were dependent on the re-formation of the cracked films, but when the predictions were in disagreement with the experimental observations of crack velocity, the propagation rate was attributed to the dissolution of the substrate at the cracked sites in the film, and was believed to be controlled by the repassivation process, which prevents dissolution. Based on the studies of many investigators, it became quite evident, however, that film formation may play an important role in SCC,[11] and that this formation may be closely associated with the surface stresses set up in the surface layer of metals and alloys.[12-14] A number of investigators have gathered experimental evidence, both direct and indirect, that hydrogen is evolved at the tip of an advancing crack during SCC of austenitic stainless steel. This evidence has been summarized and reviewed in a series of papers,[15-17] and has received renewed interest by recent investigators.[18,19]

Pertinent to the present study are the results of the X-ray investigations of SCC in austenitic stainless steel, carried out by Kamachi et al.[20] These workers preformed a Fourier analysis of the diffraction line broadening, and found that despite the small amount of plastic deformation observed in the specimens after testing, the dislocation density reached a maximum value of about 10^{11} cm^{-2}. When this value was reached, crack initiation was detected. Moreover, the stored energy--estimated from the broadening of the X-ray diffraction line--to initiate cracks was approximately the same for all specimens tested.

Of particular interest to the present study are the similarities between the susceptibility to SCC and fatigue pointed out by a number of investigators.[14,21] This interest was stimulated by the recent results of X-ray diffraction studies of cycled aluminum alloys carried out in this laboratory,[22,23] which showed that the fatigue-induced plastic deformation of the surface layer controlled the egression of dislocations from the bulk, and that upon reaching a critical density of excess dislocations in the surface layer, material failure would set in. This critical value could be predicted experimentally at a fraction of the fatigue life. Motivated by the results of these studies, the present structural investigations were undertaken. They aim to clarify the effect of the strain distribution in surface layer and bulk on the susceptibility to SCC. Tensile-deformed alloys of titanium and austenitic stainless steel, subjected to conditions of SCC, were investigated.

Although all the stress corrosion (SC) studies are still in progress and further developments are expected to emerge very soon, particularly from the studies on titanium alloys which have progressed only recently beyond the initial stages of investigation, it is felt that enough new information and corroborative evidence have been gathered to support the conclusions reached in this report.

EXPERIMENTAL PROCEDURE

Specimen Selection, Preparation and Corrosion Media

Two types of alloys were investigated: alpha-titanium and austenitic stainless steel. The nominal compositions of α-Ti alloys, designed as A_1, A_2 and A_3, were (in weight percent): Ti-5Al-5Sn-5Zr, Ti-9Al and Ti-10Al, respectively. Austenitic stainless steel, designated by A_4, was 304 commercial grade with composition Fe-18Cr-8Ni-2Mn-1Si-0.8C. All alloys were received in sheet form, and pin-loading tensile specimens were cut with the long axis parallel to the rolling direction. The selected specimen dimensions adhered to the ASTM recommendations (ASTM Standards, Part 31, A-370), with gage dimensions 1.1" x 0.05" x 0.25" (2.794 x 0.127 x 0.634 cm). Each specimen was heat-treated prior to SC testing, to stress-relieve the specimens and to obtain a uniform grain size of 20-100 μm diameter suitable for the subsequent X-ray diffraction analysis. Specimens were placed in evacuated

quartz ampules to prevent oxidation. The heat treatments, followed by water quench, are given in Table 1. After the heat treatment, the specimens were electrolytically polished. The solutions and condition of polishing are given in Table 2. To prevent oxidation and contamination effects, a surface layer of at least 100 μm was removed. Care was taken to obtain flat surfaces to satisfy subsequent testing and characterization procedures. Electropolishing was also applied for the in-depth analysis of deformation, induced by SC. Layers of micrometric dimensions could thus be removed. Two types of corrosive media were used for the α-Ti alloys A_1, A_2 and A_3. Solution I was a 0.5 aqueous, molar solution of NaCl and Solution II consisted of 0.5% HCl, 1% H_2O and 98.5% CH_3OH. Both solutions were applied at room temperature, and a wide range of cell potentials was applied during testing. The corrosive medium for austenitic stainless steel (specimen A_4) was boiling $MgCl_2$-H_2O solution at 154°C. Constant boiling temperature and $MgCl_2$ concentration were maintained by controlled heat and water flow.

TABLE 1. HEAT TREATMENT OF SPECIMENS

Alloy designation	Temperature (°C)	Time (hr)
A_1	980	10
A_2	950	3.5
A_3	950	3.5
A_4	1100	0.5

TABLE 2. POLISHING SOLUTIONS AND CONDITIONS

Alloy designation	Electrolyte	Current density A/cm^2	DC voltage	Temperature (°C)
A_1, A_2, A_3	60% methyl alcohol 34% butyl alcohol 6% perchloric acid	0.06-0.09	14	-20
A_4	60% phosphoric acid 40% sulfuric acid	$\leq$0.6	6	60

SC Testing

The SC tests were carried out at constant tensile load. An Instron Universal testing machine and a cantilever-type, dead-load machine were used for mechanical loading. To insure electrical insulation of the specimen in the solution, a special loading fixture made of Teflon was constructed. This fixture was adaptable to both testing machines. Details of the experimental arrangement are shown in Figures 1a,b. Special care was taken during the loading and unloading procedures. The rate of loading for all specimens was 0.05 in./minute (0.127 cm/minute). The corrosive media were held in a Pyrex container, and a hot plate was used for high-temperature experiments.

A Wenking potentiostat was used for adjustment of cell potential and measurements (Fig. 1).

Characterization Methods and Lattice Defect Analysis

For the routine structure characterization of the specimens, standard metallographic techniques were employed. Fracture surfaces were also investigated by scanning electron microscopy (SEM). The principal research tool, however, for structural characterization and analysis of lattice defects was the X-ray double-crystal diffractometer method in combination with X-ray topography.[24-26] On applying this method, the polycrystalline specimen is irradiated with a crystal-monochromated beam, and each reflecting grain is considered to function independently as the test crystal of a double-crystal diffractometer. The reflecting grains give rise to spot reflections which are recorded along the Debye-Scherrer arc of a cylindrical film. Depending on the perfection of the grains, the specimen is rotated in angular intervals of seconds or minutes of arc. As the grains are thus rotated through their reflecting region, discrete film shifts are carried out between each angular interval of specimen rotation. This multiple-exposure technique gives rise to an array of spots for each reflecting grain, as shown in Figures 2a-d. These arrays of spots, with their intensity dependence on specimen rotation, represent X-ray rocking curves of the reflecting grains. Thus, if the grains contain a substructure, the intensity distribution of the arrays of diffraction spots will be multipeaked, not only along the horizontal rotation direction but also along the azimuthal elevation (Fig. 2b). From the angle, subtending

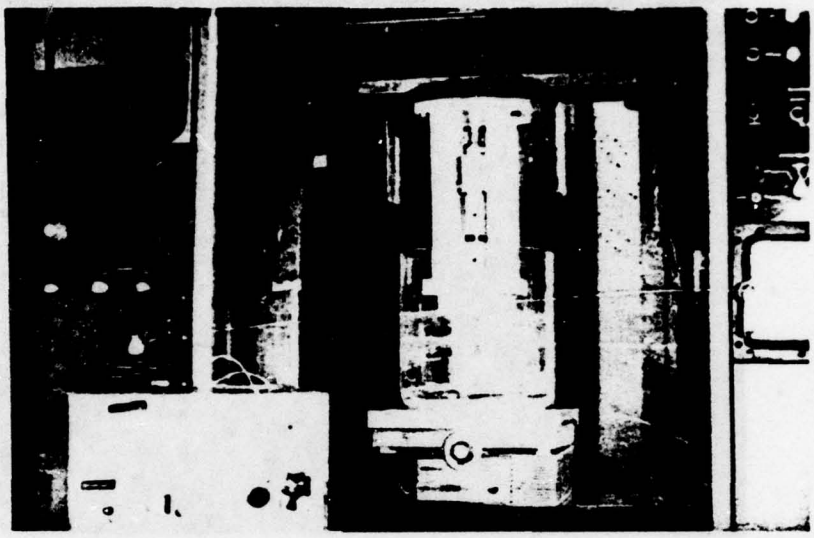

(a)

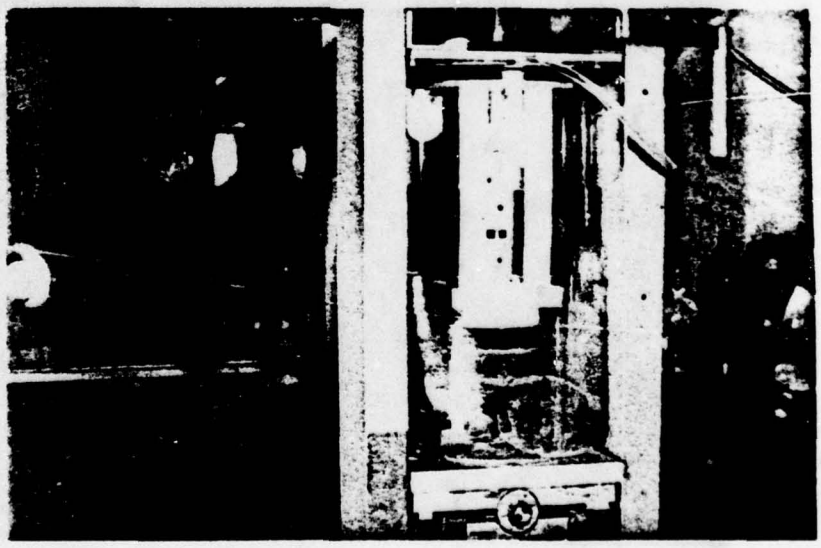

(b)

Figure 1. Experimental arrangement for specimen testing. (a) Instron Universal testing machine. (b) Cantilever dead-load machine.

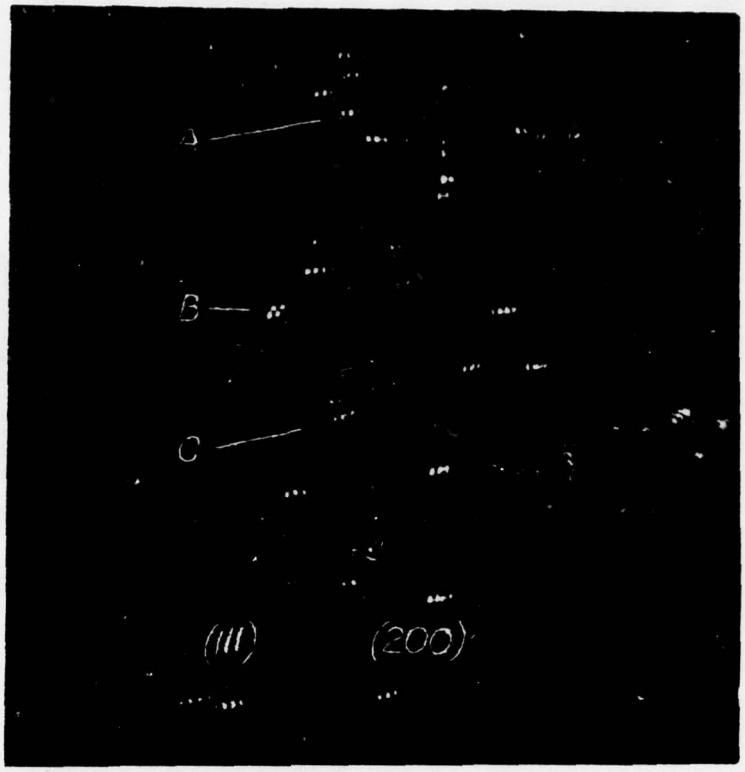

(a)

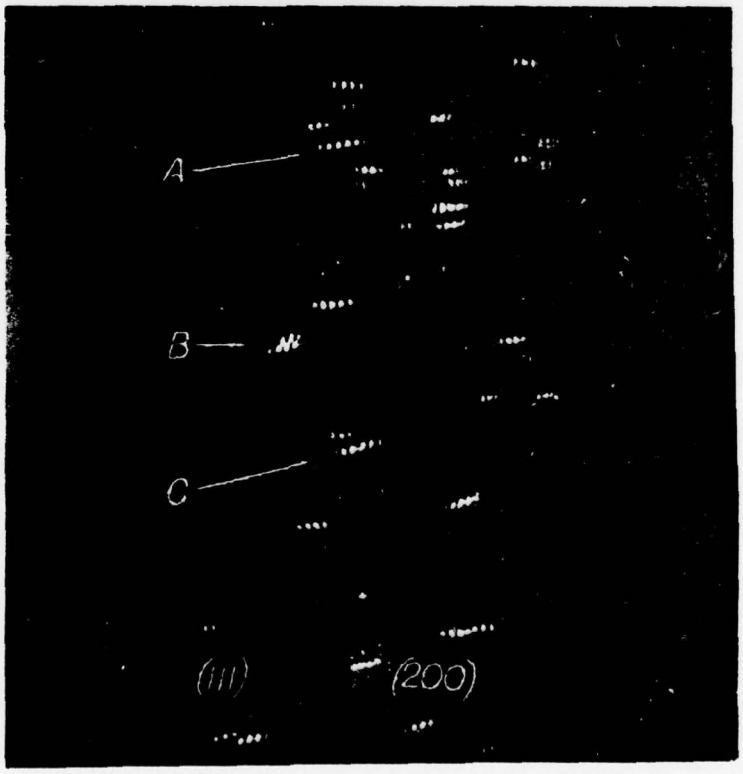

(b)

Figure 2. Detail of reflection range of identical grains. 304 austenitic stainless steel; CuK_α monochromated radiation; angular specimen setting: 6' of arc. Assigned letters establish identity of grain reflections. (a) Annealed before SC. (b) After SC at $t = 0.75\ t_c$; 55% YS.

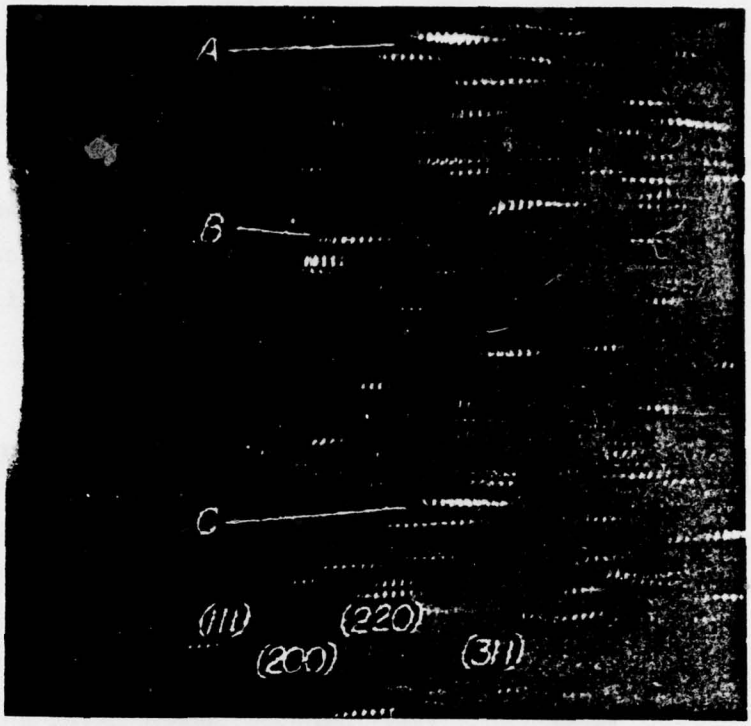

(c)

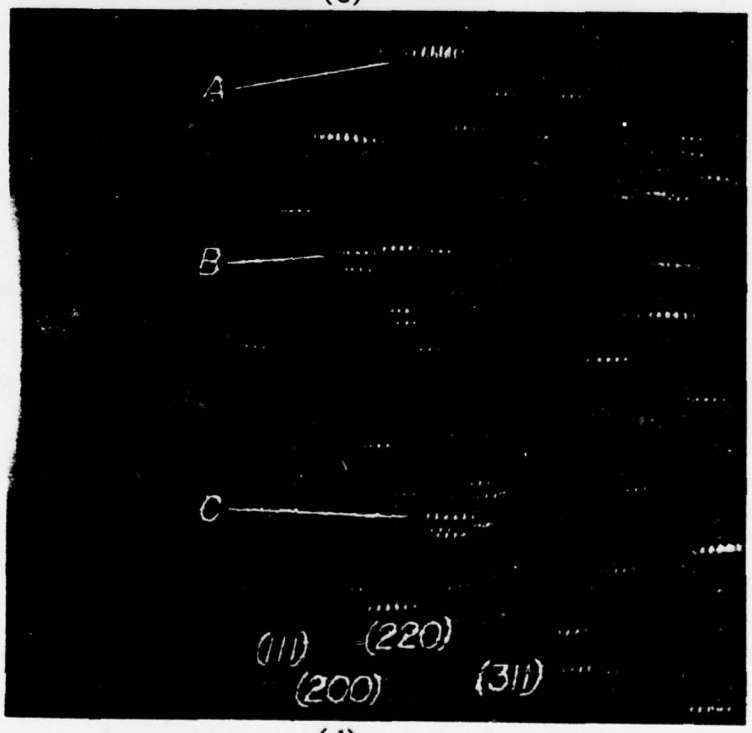

(d)

Figure 2--continued. (c) Exposed to SC, t = 0.1 t_c; 55% YS; MoK_α radiation; angular specimen setting: 3' of arc. (d) Same as (c), after removal of 100-μm surface layer.

successive peaks of the rocking curve, the excess dislocation density between subgrains can be determined, while from the spread of the subpeak curve, the excess dislocation density within the subgrain lattice can be obtained. From the width, β, at half-maximum of the rocking curve, the excess dislocation density of the entire grain is determined.[24-26] The excess dislocation density, D, is calculated from the relationship given by Hirsch:[27]

$$D = \beta^2/9b^2$$

where β is the width of the rocking curve at half of the intensity maximum (half-width) and b is the magnitude of the Burgers Vector.

By analyzing the rocking curves of the grains for various, recorded (hkl) spot reflections, a representative statistical parameter, $\bar{\beta}$, of the defect structure of the grain population is obtained. Furthermore, by taking reflection topographs (Berg-Barrett) and performing a spatial tracing of the image reflections to the spot reflections of the rocking curve, the analyzed rocking curve can be correlated to the grain topography on the specimen.

An important novel feature in the present SC study was the introduction of a precision specimen holder which permitted precise repositioning of the specimen after SC exposure or after removal of surface layers for depth profile analysis. Because a very low stress was used in the SC experiment, excessive grain rotation was avoided, and consequently, due to the precise repositioning of the specimen, the identical grain reflection could be retained. Thus the identical grains could be analyzed for their induced lattice defects as a function both of fracture time, while exposed to conditions of SC, and depth distance from the surface.

RESULTS

SC of 304 Stainless Steel

Mechanical Testing--When studies of SCC are carried out in 304 stainless steel applying a high stress in a corrosive medium such as a hot $MgCl_2$ solution, one has to consider the superposition effect of creep deformation on that caused by SC alone. Therefore, the first task of this study was to separate the creep contribution from that of SC and to establish the proper

stress level at which SCC alone would be responsible for the observable deformation process.

Control tensile tests were performed at high stress level in both argon atmosphere and non-corrosive paraffin oil at 154°C. These experiments revealed a substantial amount of creep and a drop of 35% in yield stress referred to room-temperature deformation.*

SC experiments were carried out at the three stress levels of 95, 75 and 55% YS. The dependence of fracture time on applied stress is shown in Figure 3.

It will be seen that the fracture time increased rapidly when the applied stress was dropped below the proportional limit corresponding to about 70% YS. SEM examination of the specimens stressed at 95 and 55% revealed the transcrystalline nature of the fracture mode, as shown in Figures 4a,b. Figure 5 shows the time dependence of the strain of this specimen. The small initial increase was due to elastic loading, and at the critical time t_c, when mechanical instability set in due to the development of a large central crack and concomitant reduction of cross-section, ε was about 2.5%.

In view of these mechanical and metallographic studies, it could be safely deduced that if a stress of 55% YS is applied, using $MgCl_2$ solution as the corrosive medium at 154°C, the contribution to deformation by creep can be virtually ruled out.

X-Ray Studies--X-Ray double-crystal diffractometer studies of the grain reflection were carried out as a function of corrosion time for specimens stressed at 55% YS. Figure 2a shows details of the rocking curves of reflecting grains of an annealed specimen before SC exposure. Figure 2b shows the effect of SC exposure at $t = 0.75\ t_c$ on the rocking curves of identical grains. It will be seen that due to plastic deformation the angular rotation of the grain reflection has increased. Furthermore, the induced plastic deformation of the grain is manifested by a breakup of the spot reflections with sequential intensity maxima and minima that are characteristic of a deformation substructure.[24,25] Figures 2c,d show the effect of surface removal on the rocking curve of the identical grain and concomitant decrease of reflection

*The applied stress level in the SC experiments will be given in percent yield stress (% YS) referred to room-temperature deformation.

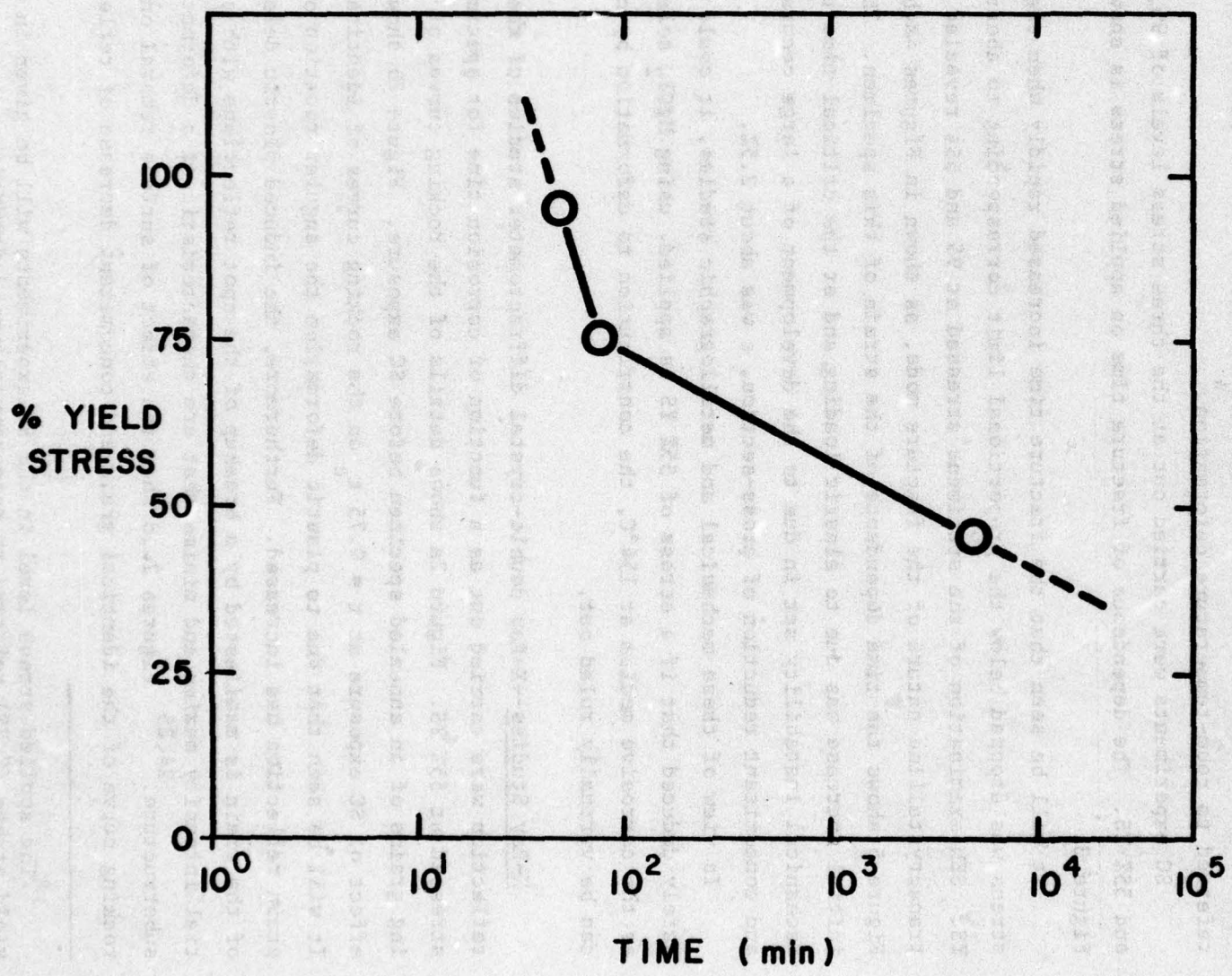

Figure 3. Dependence of fracture time on applied stress. 304 austenitic SS.

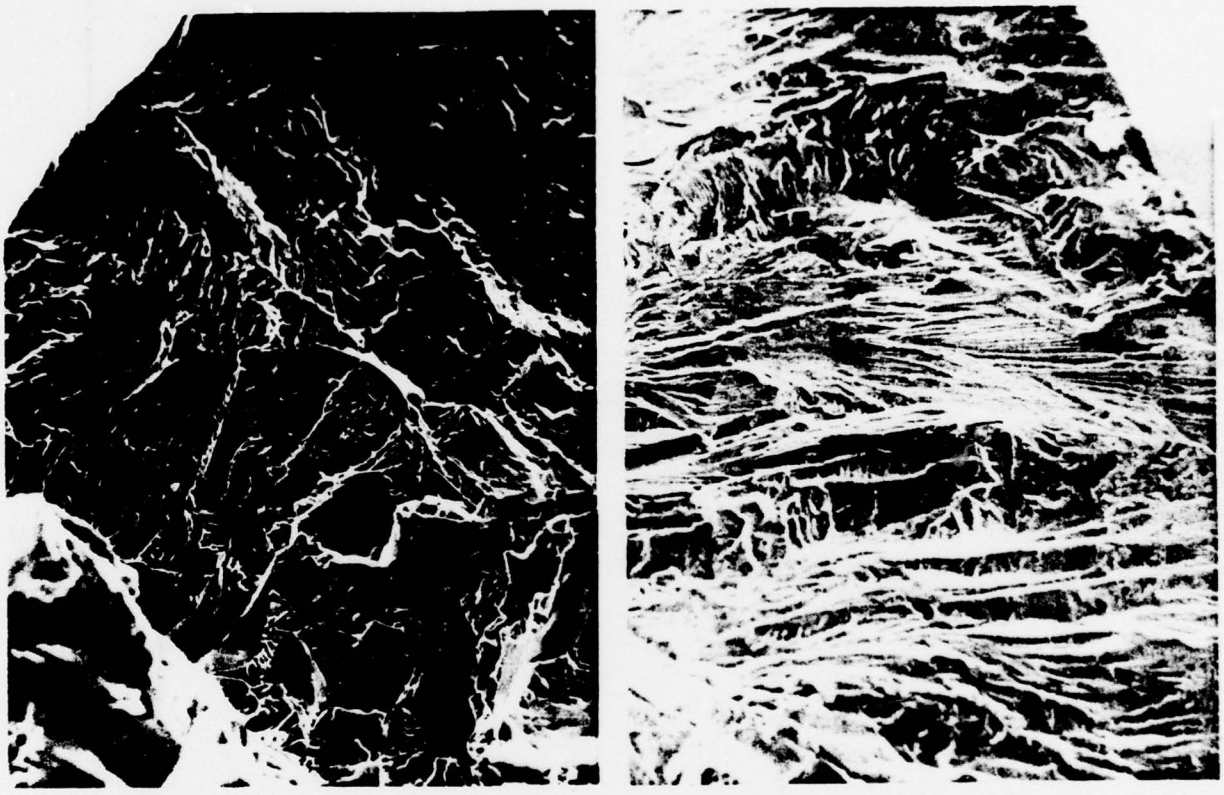

(a) (b)

Figure 4. SEM fractograph of 304 austenitic SS. (a) 95% YS; 200X. (b) 55% YS; 200X.

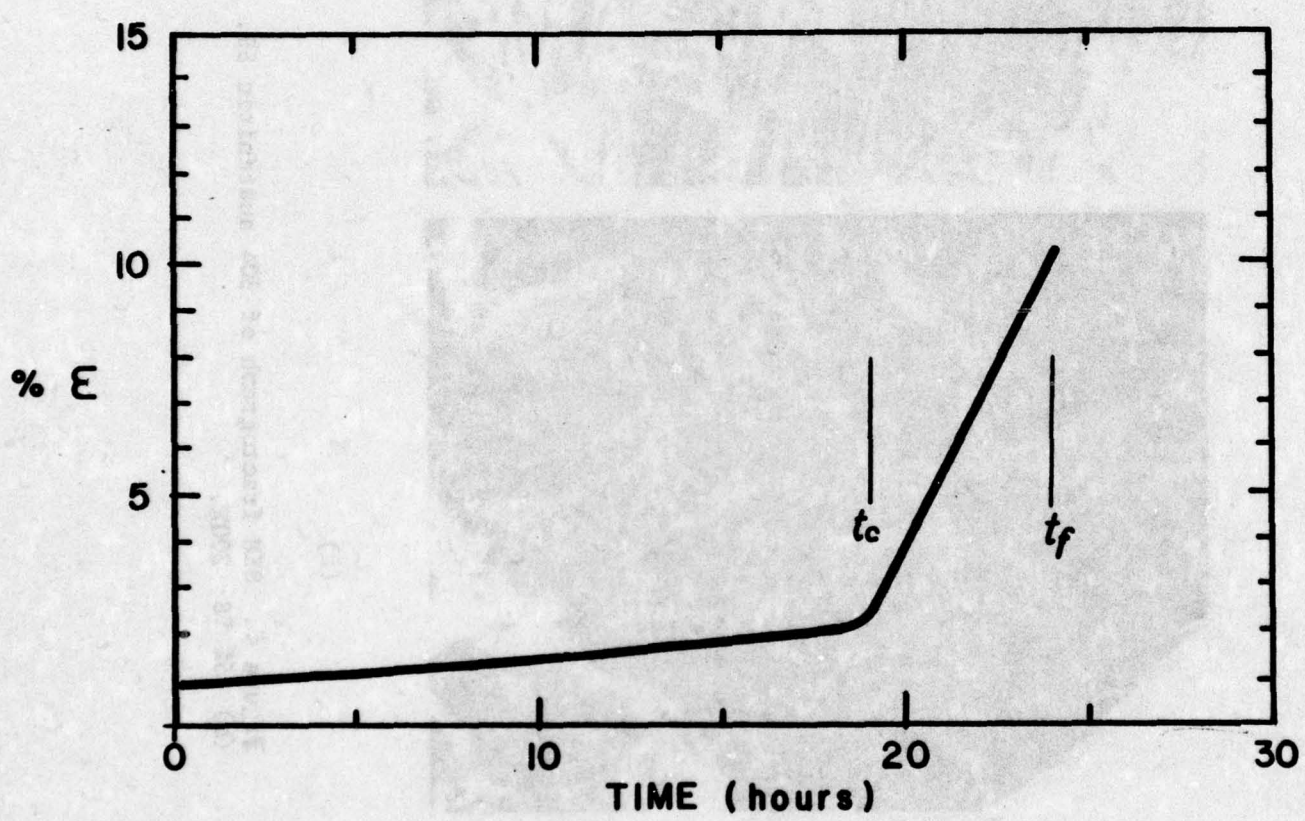

Figure 5. Time dependence of strain. 304 austenitic SS; 55% YS.

range for t = 0.1 t_c, employing MoK_α radiation. Figure 6 shows the dependence of the average, normalized half-width of the rocking curve β/β_o on t, where β_o refers to the average half-width of the annealed specimen prior to SC exposure. β/β_o retained the value of unity in control experiments, when the specimens had either the same stress level without exposure to the corrosive medium, or were exposed to the medium without applied stress.

Figure 6 displays two curves. The lower curve, A, refers to the average β/β_o values of all grain reflections analyzed and, therefore, expresses the mean dependence of lattice distortions induced in the grains by SC.

It will be remembered that for a low applied stress, the rocking curves of identical grains can be analyzed. It was observed that certain grains showed a persistent increase of the angular range of reflections with t, and that the topographic images of the reflections exhibited image contrast of lattice distortions resulting from dislocation interaction. The upper curve of Figure 6, B, represents the β/β_o values of these specific grain reflections. Hence curve B is a more representative indication of the lattice distortions induced by SC, since it is composed of β/β_o values derived from grains selectively affected by SC. Both curves ascend to maximum values at the critical corrosion time of t_c ~ 19.5 hours, after which they decline conspicuously. The maxima of β/β_o are 2.40 and 1.64 for the upper and lower curve, respectively. For this stress level, t_c corresponds to about 80% of the total failure time, t_f, and corresponds to the onset of the macroscopic mechanical instability shown in the ε-t curve of Figure 5. The macroscopic, mechanical instability from t_c to t_f is reflected on a microscopic scale by the rapid rise of β/β_o, shown in Figure 6.

To study the effects of SC with depth distance from the surface, rocking curves of identical grain reflections were analyzed by successive removal of surface layers through etching. Thus, a profile of β/β_o values as a function of depth distance was obtained, such as that shown in Figure 7, for a specimen stressed to 55% YS and exposed to the corrosive medium of 0.1 t_c. For depth profile studies, the application of CuK_α radiation proved to be very useful, because for this radiation the mass absorption coefficient for steel is very high, so that the average path of depth penetration of the probing X-ray beam was about 1 μm. The concomitant fluorescent radiation was easily controlled by the combined effects of the monochromated radiation reflected from the

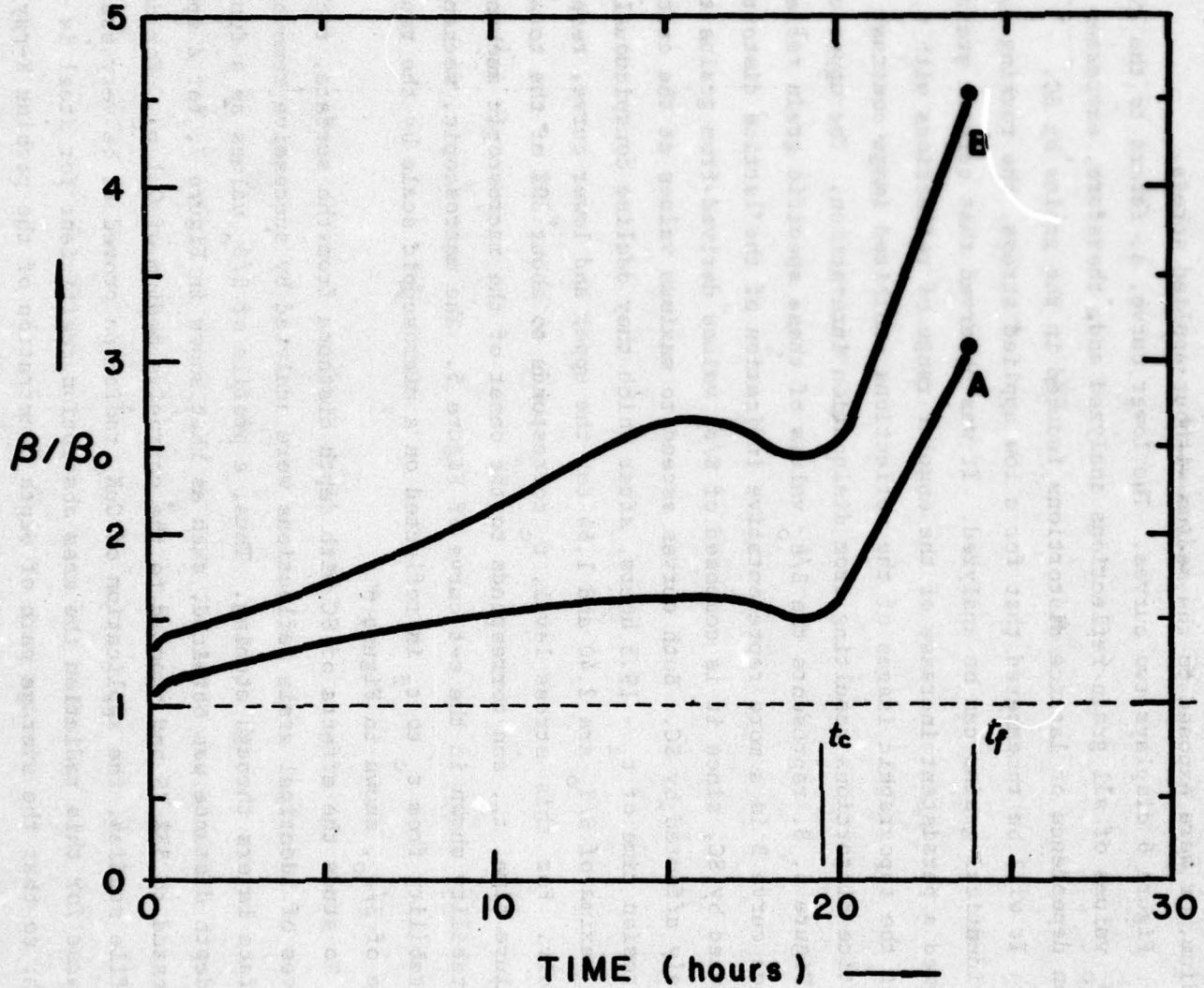

Figure 6. Normalized rocking curve half-width, β/β_o, as a function of SC time. A is mean β/β_o of all analyzed grain reflections. B is β/β_o of selective grain reflections.

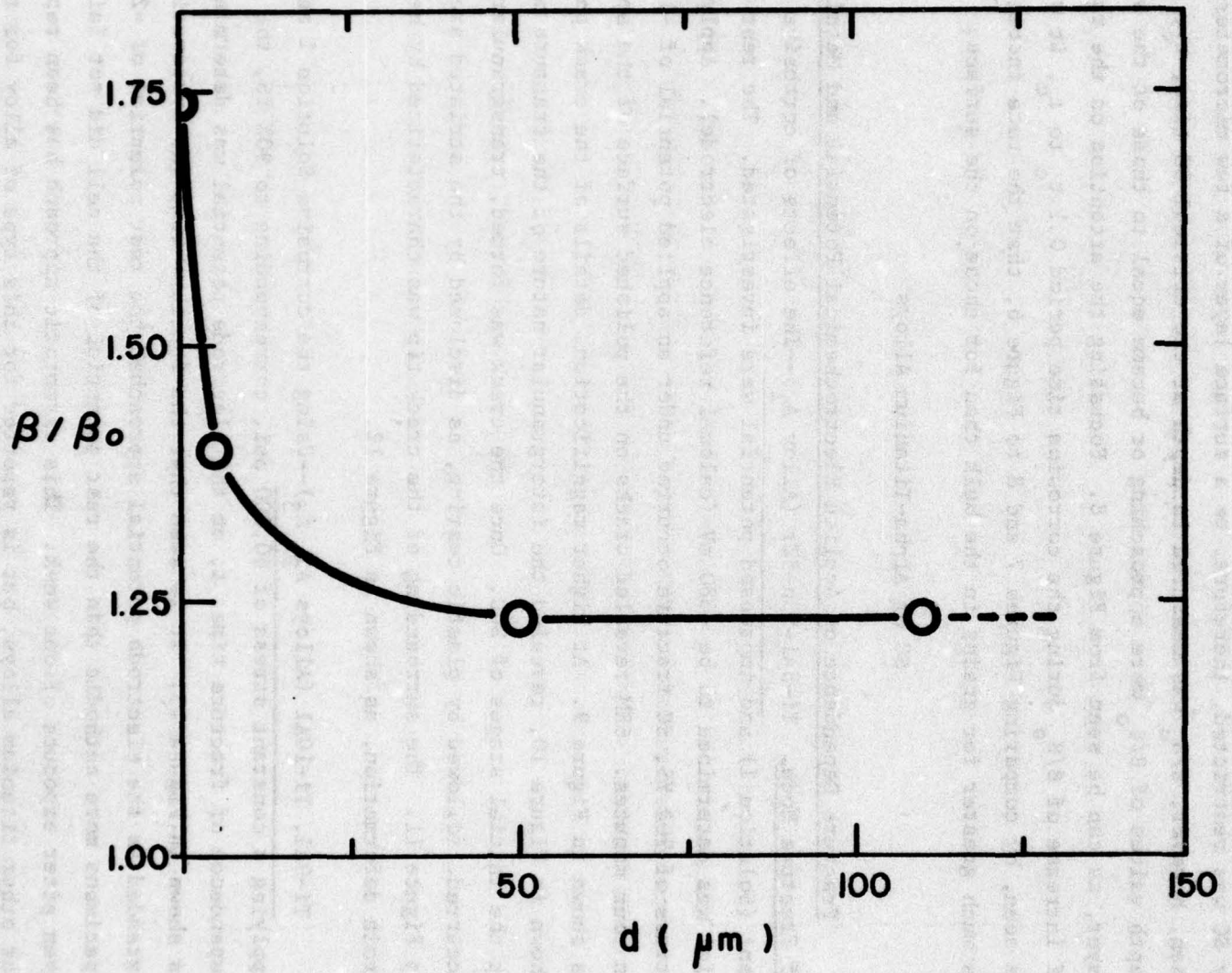

Figure 7. Profile of β/β_o as a function of depth distance from surface, d. 55% YS; $t = 0.1\ t_c$.

analyzing crystal and by application of multiple films or interposed screens which absorbed the fluorescent radiation.

It will be seen from Figure 7 that the β/β_o value at the surface was about 40% larger than in the bulk, and that the plastic deformation induced by SC was restricted, therefore, to a surface layer of a few micrometers. When, however, β/β_o was measured in depth at the critical SC time, t_c, the depth values of β/β_o were approaching or became equal to those of the surface layer, as can be seen from Figure 8. Focussing the attention on the rate of increase of β/β_o during the corrosion time period 0.1 t_c to t_c, it will be seen, by comparing Figures 7 and 8 to Figure 6, that the rate increase is much greater for grains in the bulk than for those on the surface.

SC of Alpha-Titanium Alloys

Fracture Dependence on Applied Electrochemical Potential and Metallography of Fracture Mode. Ti-5Al-5Sn-5Zr (Alloy A_1)--The effects of corrosive environment (Solution I) and impressed potential were investigated. The rest potential was determined to be -380 mV (calomel reference electrode). Applying a stress of 90% YS, SC fracture occurred under an applied potential of -100 mV in four minutes. SEM revealed cracks on the polished surface of the specimen, as shown in Figure 9. At higher magnification, details of the crack path, shown in Figure 10, revealed the intergranular nature of the fracture mode at the initial stages of SCC. Once the crack was formed, transgranular fracture occurred, followed by plastic tearing, as disclosed by the striated areas shown in Figure 11. The surrounding of the crack tip was characterized by heavy grain deformation, as shown in Figure 12.

Ti-9Al, Ti-10Al (Alloys A_2, A_3)--Using the corrosive Solution I and applying a constant stress of 60,000 psi, corresponding to 90% YS, the dependence of fracture time, t, on the electrode potential was determined and is shown in Figure 13. It is seen that the fracture time was systematically extended as the electrode potential approached the rest potential of -230 mV. Specimens more cathodic than the rest potential of the cell did not fail, even after exposure of one week. This asymptotic approach has been reported for other titanium alloys, but is reported for this type of alloy for the first time.

Figure 8. Profile of β/β_o as a function of depth distance from surface, d. 55% YS; $t = t_c$.

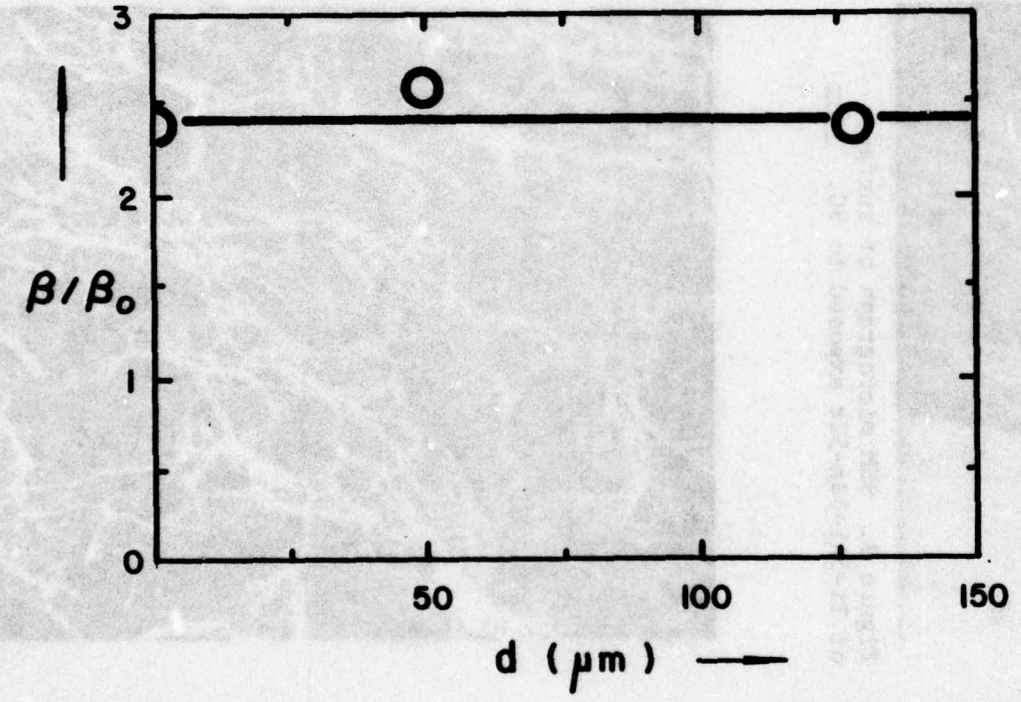

Figure 9. SEM micrograph of surface of Ti-5Al-5Sn-5Zr exposed to SC. 150X.

Figure 10. Intergranular cracking in Ti-5Al-5Sn-5Zr. 700X.

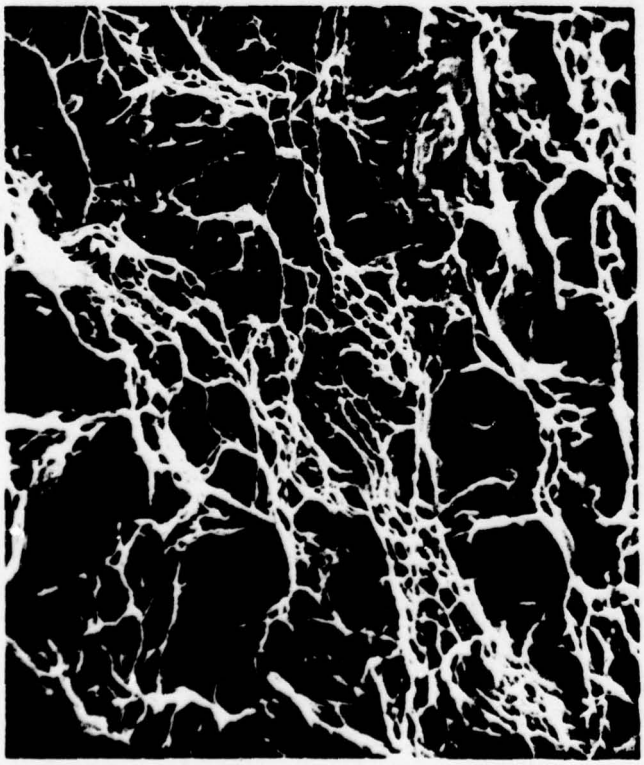

Figure 11. Transgranular fracture path in Ti-5Al-5Sn-5Zr. 700X.

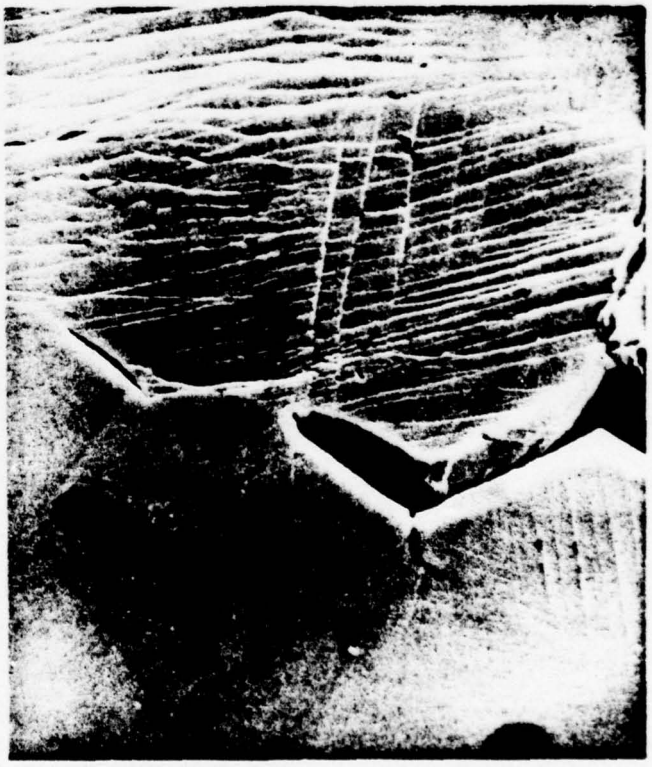

Figure 12. Grain deformation at crack tip of Ti-5Al-5Sn-5Zr. 2000X.

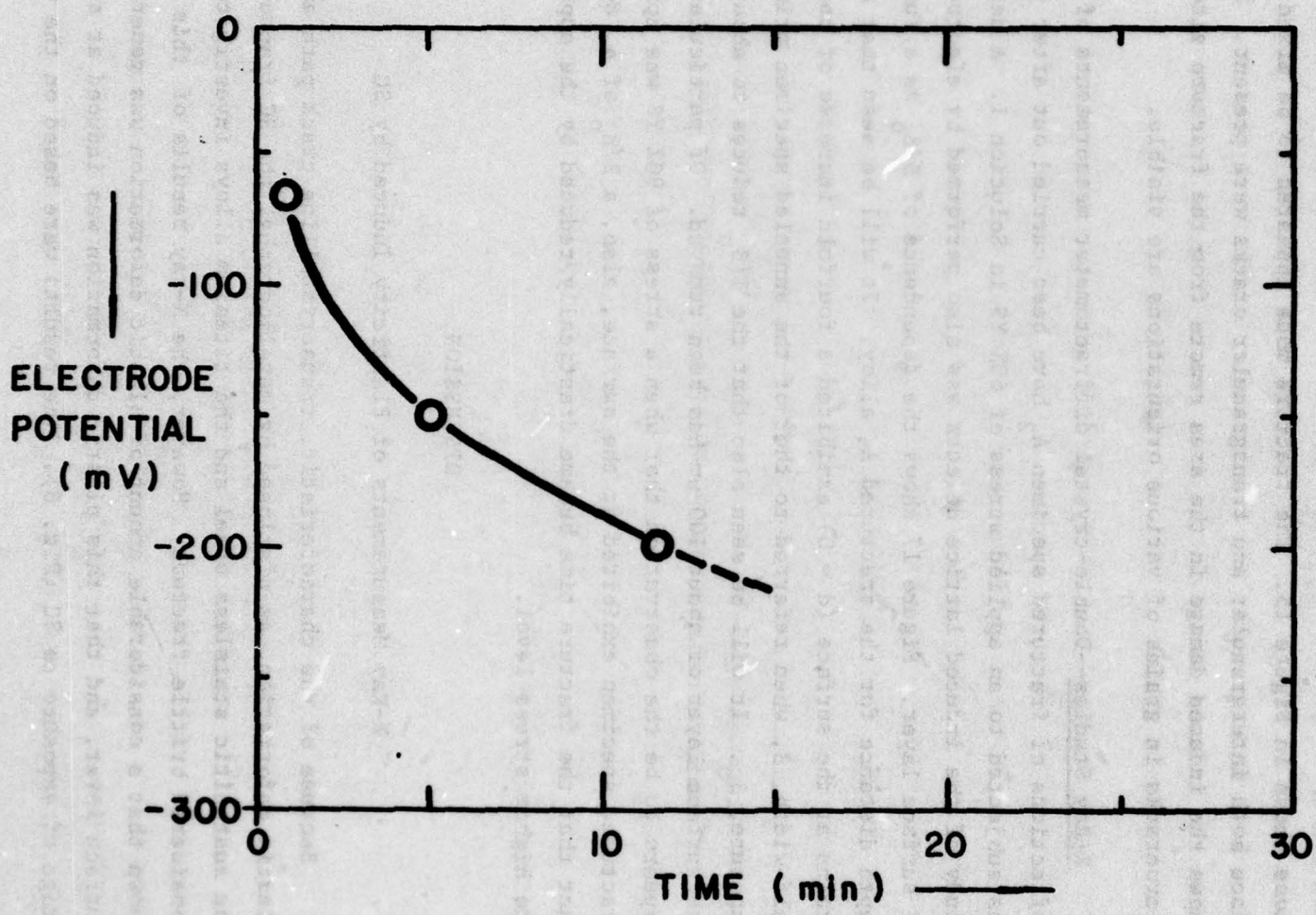

Figure 13. Dependence of fracture time on impressed potential. Ti-9Al; 90% YS.

The effect of applied stress on fracture time was also investigated, keeping the imposed potential of -200 mV constant. It may be seen from Figure 14 that the reduction of the stress level from 90% YS (60,000 psi) to 60% YS (40,000 psi) increased the fracture time by a factor of four. Metallographic studies revealed typical SC cracks at the fracture site, like those shown in Figure 15. The fracture mode appeared to be mixed in nature, since both intergranular and transgranular cracks were present. Figure 16 shows the induced damage in the area remote from the fracture site. Many microcracks in grains of various orientations are visible.

X-Ray Studies--Double-crystal diffractometer measurements of grain reflections of fractured specimen A_2 have been carried out after the specimen was subjected to an applied stress of 60% YS in Solution I. A depth profile study of the induced lattice defects was also performed by electrolytic removal of surface layer. Figure 17 shows the dependence of β/β_o as a function of depth distance for the fractured A_3 alloy. It will be seen that selective grains at the surface (d = 0) exhibited a fourfold increase of rocking curve half-width, β, when referred to that of the annealed specimen prior to SC exposure, β_o. It will be seen also that the β/β_o reduces to about 2 after the surface layer of about 100 μm has been removed. Of particular significance appears to be the observation that when a stress of 90% YS was applied, the fractured specimen exhibited at the surface, also, a β/β_o of 4, despite the fact that the fracture time became drastically reduced by the application of the higher stress level.

DISCUSSION

X-Ray Measurements of Plasticity Induced by SC

Because of the characteristic, transcrystalline crack path and small plastic deformation, as disclosed by metallography, the SC fracture of both the austenitic stainless steel and the titanium alloys investigated can be considered brittle fracture. However, the X-ray results of this study have shown that a considerable amount of plastic deformation was generated in the surface layer, and that this plastic deformation was induced at an early stage of exposure to SC (Fig. 6). The results were based on the measurements

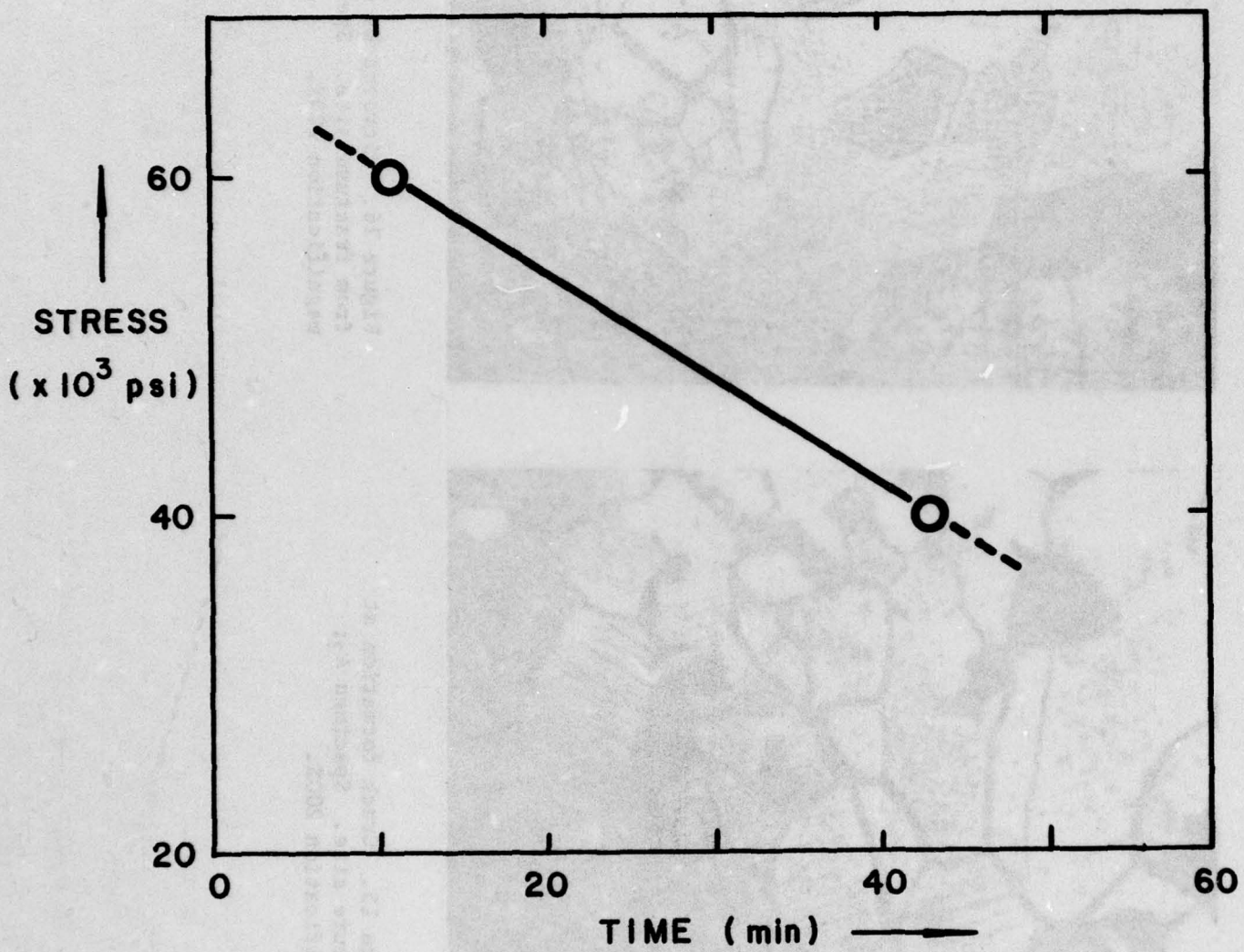

Figure 14. Effect of applied stress on fracture time. Ti-9Al; -200 mV.

Figure 15. Crack formation at fracture site. Specimen A_3; magnification 200X.

Figure 16. Microcracks remote from fracture site. Specimen A_3; magnification 200X.

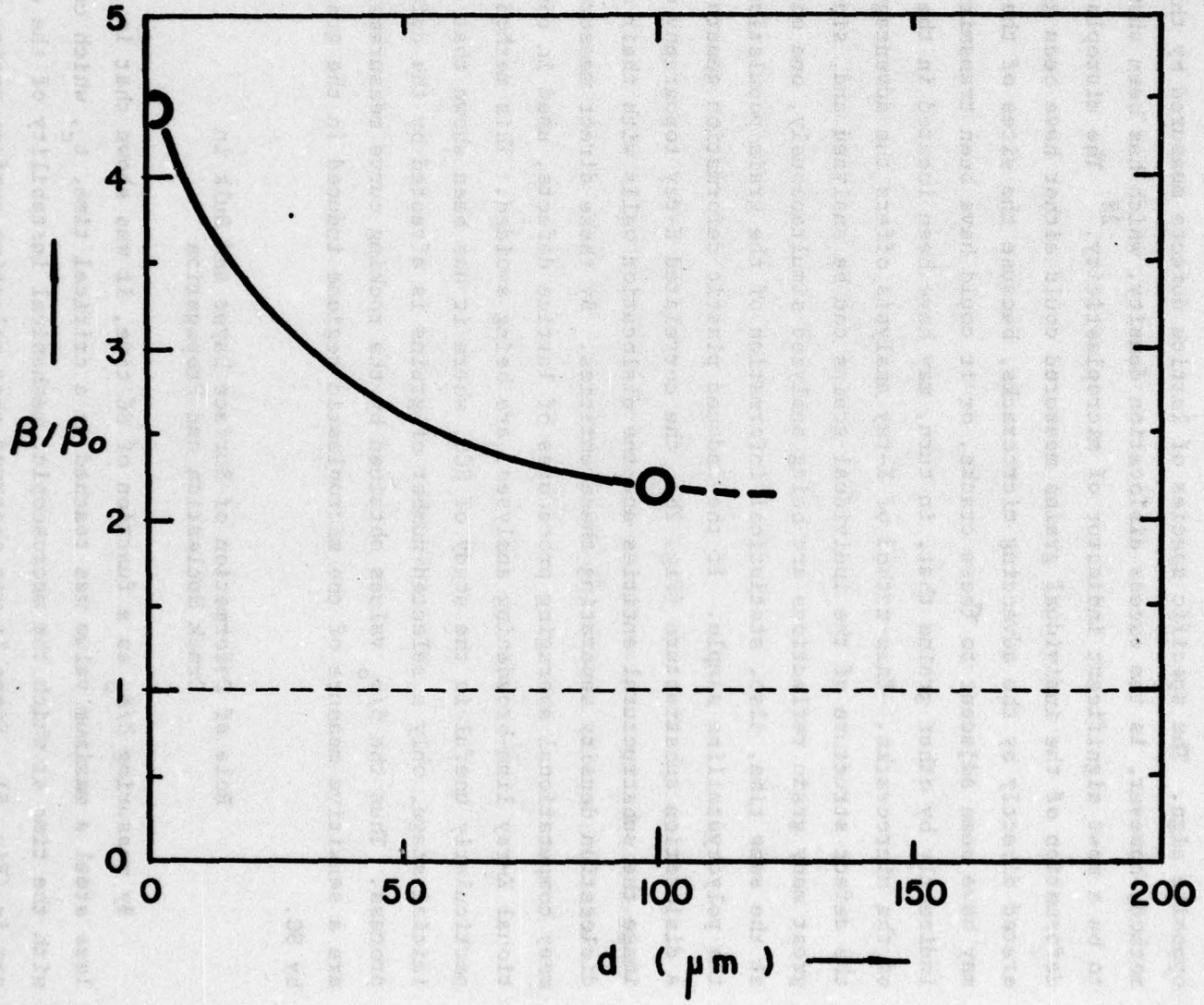

Figure 17. Dependence of β/β_o on removal of surface layer. Specimen A_3; 60% YS; -200 mV.

of the increase of the angular range of reflections of the grains, β/β_o, and analysis of the topography of the corresponding reflection images.

The measurements of the rocking curve half-widths that were carried out do not give information about groupings of adjacent dislocations of opposite sign. The specific species of lattice defects measured by this method, however, is the excess dislocation density, which has been shown to be a most significant indicator of microplasticity.[28] The microplastic deformation of the individual grains measured could either have been generated directly by the advancing microcracks, because the sites of the grains may have been adjacent to these cracks, or it could have been transmitted indirectly by other grains that, in turn, may have been located in the vicinity of the microcracks. This method of X-ray analysis offers the advantage that the defect structure of the individual grains can be analyzed and, since a great many grain reflections are being analyzed simultaneously, one obtains at the same time, also, statistical information of the grain population of the polycrystalline sample. If the induced plastic deformation generates a dislocation substructure (Fig. 2b), the correlated X-ray topography will image the substructural entities and the dislocation walls with their excess dislocation density separating these entities. By these direct measurements, many computational averaging procedures of lattice defects, used in conventional X-ray line-broadening analyses, are being avoided. This method is particularly useful in the study of SCC, where it has been shown that in the initial stage, only a selected number of grains is affected by the deformation process. Thus the β/β_o values obtained by the rocking curve measurements are a sensitive measure of the microplastic regions induced in the grains by SC.

Role of Deformation of Surface Layer and Bulk in Crack Nucleation and Propagation

By measuring β/β_o as a function of SC time, it was shown that in 304 stainless steel a maximum value was reached at a critical time, t_c, which coincided with the time at which the macroscopic, mechanical instability of the alloys set in (Fig. 5). Since it was observed that selective surface grains exhibited a persistent increase of lattice defects with exposure time (curve B, Fig. 6), it appears reasonable to deduce that the SC process affected selectively those

grains that, because of their orientation and constraints, underwent the greatest amount of plastic deformation.

The depth profile studies of induced lattice defects disclosed, in both stainless steel and titanium alloys, that the preferential plastic deformation at the surface created a barrier effect with respect to the egression of excess dislocations generated in the bulk. The same effect was shown in statically and cyclically deformed, commercial aluminum alloys.[22,23] In aluminum and titanium alloys the plastically deformed surface layer extended to about 100 μm (Fig. 17), but in stainless steel it comprised only a few micrometers (Fig. 7).

In SC the electrochemical attack was not only initiated at the surface by the preferential plastic deformation of the surface layer, but sustained by the progressive deformation of the surface layer with fracture time. As in fatigue of metals,[22,23] one also encounters in SC a buildup of dislocation density in the bulk of the material with time. Just as in fatigue, there exists also in SC a dynamical interplay between the buildup of excess dislocations in the surface and bulk. During the initial stage of SC, e.g. from $t = 0$ to $t = 0.1\ t_c$, there was a rapid rise of excess dislocations in the surface layer but only a minimal increase in the bulk, as may be seen by comparing the β/β_o values of Figure 6 to those of Figure 7. During the SC time period from $0.1\ t_c$ to t_c, the rate increase of excess dislocations for the grains located in the bulk was much greater than for the surface grains (compare Figs. 7 and 8 to Fig. 6). This steeper increase in the bulk has to be attributed to the effective blocking effect to dislocation egression by the surface layer.

In SC the chemical corrosion process is superimposed and is aided by the dislocation dynamics between surface and bulk. One can conceive, therefore, that the electrochemical attack was initiated at the plastically deformed, film-free metal grains functioning as anode, while the undistorted grains functioned as the cathode in a galvanic cell. Microcracks could be initiated, therefore, which would advance by a combination of electrochemical and mechanical action.[2,29] The diffusion of the chemical attacking species from the surface region to the bulk is presumably assisted by the intense dislocation activity in the surface layer.[19,30] Thus the surface layer in SC is subjected simultaneously to two opposing effects: one is due to the

preferential work-hardening with respect to the bulk, which confers to the surface layer the property of a barrier against the egression of dislocations generated in the bulk; the other is due to the electrochemical attack which embrittles the surface layer, the more so as the dislocation activity of the former effect is increased. This corrosive embrittlement of the surface layer lowers the critical β value when compared to a stressed material in a non-corrosive medium. When the resistance of the surface layer toward the egression of dislocations from the bulk is lowered to a critical value, $(\beta/\beta_o)^*$, macroscopic mechanical instability will set in with concomitant rapid crack propagation. Such a stage was reached at the fracture time t_c of Figure 6.

It should be pointed out that the discrepancy between the observed crack velocities and the predictions derived from the various proposed theories of SC constituted one of the most disputed stumbling blocks to bringing theory and experimental observations in agreement. The concept, however, of the dynamical interaction of deformed surface layer and bulk under chemical corroion and the eventual breakdown of surface layer resistance when the accumulated excess dislocations have reached a critical value, β^*, appears to offer a satisfactory solution to this dilemma. The criticality of β^* in SCC found in this study is in agreement with the X-ray results reported by Kamachi et al.[20]

Experimental Prediction of SC Lifetime

The results of the studies imply that the critical accumulation of excess dislocations in the surface layer, experimentally determined by β^*, governs the fracture of the material. In both austenitic steel and alpha-titanium alloys, mechanical instability occurred when β^* was approached, regardless of whether the route to fracture was taken by application of high stress and short SC exposure time or low stress and long SC exposure time. The recognition of the importance of β^* in SCC opens up the exciting vista that the lifetime of an alloy, subjected to conditions of SC, can be predicted experimentally if the measured average half-width value of the alloy, $\bar{\beta}$, can be expressed at a specific SC time, t, as a ratio of $(\beta/\beta_o)^*$.

Inspection of curve A of Figure 6 will show that the slope in the plot β/β_o vs t is rather shallow and that, therefore, $\bar{\beta}$ cannot be expressed in

terms of $(\beta/\beta_o)^*$ with any degree of certainty, since any measured $\overline{\beta}$ value would fall within the experimental error band. The failure to predict SC lifetime from such a curve stems from the fact that the X-ray measurements of curve A included the analyses of many grains that were not appreciably affected by the SC attack, and hence suppressed the effect of SC on the broadening of the rocking curve width. This explains why conventional X-ray line-broadening analyses have not been effective in predicting the SC lifetime.

By contrast, curve B of Figure 6 exhibits a steeper ascent, and hence by constructing a calibration curve and its error band, $\overline{\beta}$ can be expressed in terms of $(\beta/\beta_o)^*$. The possibility of predicting SC time based on curve B derives from the fact that the double-crystal diffractometer method, employed in this study, was capable of distinguishing those grains that exhibited pronounced susceptibility to SC, by virtue of the broadening of their rocking curves, from those which did not. The latter grains could thus be excluded from the statistical count.

In addition to predicting $(\beta/\beta_o)^*$ from selective grain reflections of the surface layer, there exists the distinct possibility, as the depth profile analyses of Figures 7 and 8 have shown, that $(\beta/\beta_o)^*$ can be predicted from a calibration curve of β/β_o vs t of grain reflections emanating from the bulk. Such a calibration curve can be prepared from a series of alloy specimens subjected to identical conditions of SC, from which, at various time intervals, a surface layer of about 150 μm has been removed prior to each X-ray analysis. Removal of the surface layer prior to each analysis is necessary to insure grain representation from the bulk. Construction of such a calibration curve is currently in progress.

This phenomenon of gradual buildup of excess dislocation in the bulk in SCC appears to be analogous to recent results obtained from studies of fatigued aluminum alloys carried out in this laboratory. In the latter studies it was also shown that the accumulation of the lattice defects generated by cycling occurred very rapidly in the surface layer, while in the bulk the buildup was more gradual. For these cycled alloys a linear relationship was obtained between β/β_o and number of cycles to failure, with a measurable slope to predict $(\beta/\beta_o)^*$ experimentally.[22,23]

CONCLUSIONS

Lattice defects induced by SC of 304 austenitic stainless steel and titanium-aluminum alloys were investigated by a method based on X-ray double-crystal diffractometry combined with X-ray topography. X-Ray rocking curves of grain reflections from surface layer and bulk were obtained, and from the population of the grain reflections a statistical half-width value of the rocking curves, $\bar{\beta}$, was derived. This $\bar{\beta}$ value was a measure of the excess dislocation density of the analyzed grains. The following results were obtained:

1. Selective grains at the surface exhibited a pronounced susceptibility to SC with concomitant increase of their β values, while under conditions of stress application alone or corrosive medium without stress, the β values remained unaltered.
2. The excess dislocation density of the surface grains, suceptible to SC, increased with SC time until a critical value $\bar{\beta}^*$ was reached at a SC time, t_{cr}, at which macroscopic mechanical instability set in.
3. Investigation of the induced excess dislocations in depth showed that there exists a dynamical interplay between the buildup of excess dislocations in the surface and bulk.
4. During the initial stage of SC in 304 stainless steel ($t = 0$ to $t = 0.1\ t_{cr}$), there was a rapid rise of excess dislocations in the surface layer but only a minimal increase in the bulk.
5. Up to $\bar{\beta}^*$, the surface layer functioned as a barrier to the egression of excess dislocations from the bulk. Due to this barrier effect, the excess dislocation density in the bulk increased until at t_c it was virtually equal to that on the surface.
6. Predictions of SC time of alloys can be made by the non-destructive X-ray double-crystal diffractometer method, if calibration curves are prepared based on the $\bar{\beta}$ values of grain reflections from surface and bulk.

REFERENCES

1. Pugh, E. N., Environment-Sensitive Mechanical Behavior, Gordon and Breach, 1965, p. 351.
2. Hoar, T. P., and Hines, J. G., Stress Corrosion Cracking and Embrittlement, John Wiley and Sons, New York, 1956, p. 107.
3. Sanderson, G., and Scully, J. C., Corrosion Sci., 8, 541 (1968).
4. Powell, D. T., and Scully, J. C., Corrosion, 24, 453 (1968).
5. Coleman, E. G., Weinstein, D., and Rostocker, W., Acta Met., 9, 491 (1961).
6. Powell, D. T., and Scully, J. C., Corrosion, 25, 483 (1969).
7. Scully, J. C., and Powell, D. T., Corrosion Sci., 10, 371 (1970).
8. Logan, H. L., J. Research, NBS, 48, 99 (1952).
9. Forty, A. J., and Humble, P., Phil. Mag., 8, 247 (1963).
10. McEvely, A. J., and Bond, A. P., J. Electrochem. Soc., 112, 131 (1965).
11. Staehle, R. W., Proc. Int. Conf. on Stress Corrosion Cracking and Hydrogen Embrittlement of Iron-Base Alloys, Firminy, France, June 1973, NACE.
12. Kramer, I. R., and Podlasek, S., Acta Met., 11, 70 (1963).
13. Kramer, I. R., and Kumar, A., Trans. TMS-AIME, 3, 1223 (1972).
14. Kramer, I. R., Corrosion, 31, 383; ibid., 391 (1975).
15. Staehle, R. W., The Theory of Stress Corrosion Cracking in Alloys (ed. J. E. Scully), NATO, Brussels, 1971, p. 223.
16. Theu, G. J., and Staehle, R. W., Proc. Int. Conf. on Stress Corrosion Cracking and Hydrogen Embrittlement of Iron-Base Alloys, Firminy, France, June 1973, NACE.
17. Asaro, R. J., West, A. J., and Tiller, W. A., Proc. Int. Conf. on Stress Corrosion Cracking and Hydrogen Embrittlement of Iron-Base Alloys, Firminy, France, June 1973, NACE.
18. Mehta, M. L., and Burke, J., Corrosion, 31, 108 (1975).
19. Sudarshan, T. S., Louthan, M. R. Jr., and McNitt, R. P., Scripta Met., 12, 79 (1978).
20. Kamachi, K., Otsu, T., and Obayashi, S., J. Japan Inst. Metals, 35(12), 64 (1971).

21. Schlain, D., Bur. Mines Bull. 619, U.S. Dept. of the Interior (1964).

22. Pangborn, R. N., Weissmann, S., and Kramer, I. R., Scripta Met., 12, 129 (1978).

23. Pangborn, R. N., Ph.D. Thesis, Rutgers University, New Brunswick, N. J., 1979.

24. Weissmann, S., and Evans, D. L., Acta Cryst., 7, 733 (1954).

25. Weissmann, S., J. Appl. Phys., 27, 389 (1956).

26. Weissmann, S., Trans. ASM, 52, 599 (1960).

27. Hirsch, P. B., Prog. Met. Phys., 6, 283 (1956).

28. Tsuneskawa, Y., and Weissmann, S., Met. Trans., 5, 1585 (1974).

29. Whitwham, D., and Evans, U. R., J. Iron Steel Inst., 165, 72 (1950).

30. Louthan, M. R. Jr., Caskey, G. R., Donavan, J. A., and Rawl, D. E. Jr., Mat. Sci. Eng., 10, 357 (1972).

BASIC DISTRIBUTION LIST

Technical and Summary Reports April 1978

Organization	Copies
Defense Documentation Center Cameron Station Alexandria, VA 22314	12
Office of Naval Research Department of the Navy 800 N. Quincy Street Arlington, VA 22217	
ATTN: Code 471	1
Code 102	1
Code 470	1
Commanding Officer Office of Naval Research Branch Office Building 114, Section D 666 Summer Street Boston, MA 02210	1
Commanding Officer Office of Naval Research Branch Office 536 South Clark Street Chicago, IL 60605	1
Office of Naval Research San Francisco Area Office One Hallidie Plaza Suite 601 San Francisco, CA 94102	1
Naval Research Laboratory Washington, DC 20375	
ATTN: Codes 6000	1
6100	1
6300	1
6400	1
2627	1
Naval Air Development Center Code 302 Warminster, PA 18964 ATTN: Mr. F. S. Williams	1

Organization	Copies
Naval Air Propulsion Test Center Trenton, NJ 08628 ATTN: Library	1
Naval Construction Batallion Civil Engineering Laboratory Port Hueneme, CA 93043 ATTN: Materials Division	1
Naval Electronics Laboratory San Diego, CA 92152 ATTN: Electron Materials Sciences Division	1
Naval Missile Center Materials Consultant Code 3312-1 Point Mugu, CA 92041	1
Commanding Officer Naval Surface Weapons Center White Oak Laboratory Silver Spring, MD 20910 ATTN: Library	1
David W. Taylor Naval Ship Research and Development Center Materials Department Annapolis, MD 21402	1
Naval Undersea Center San Diego, CA 92132 ATTN: Library	1
Naval Underwater System Center Newport, RI 02840 ATTN: Library	1
Naval Weapons Center China Lake, CA 93555 ATTN: Library	1
Naval Postgraduate School Monterey, CA 93940 ATTN: Mechanical Engineering Department	1

BASIC DISTRIBUTION LIST (cont'd)

Organization	Copies
Naval Air Systems Command Washington, DC 20360 ATTN: Codes 52031 52032	1
Naval Sea System Command Washington, DC 20362 ATTN: Code 035	1
Naval Facilities Engineering Command Alexandria, VA 22331 ATTN: Code 03	1
Scientific Advisor Commandant of the Marine Corps Washington, DC 20380 ATTN: Code AX	1
Naval Ship Engineering Center Department of the Navy Washington, DC 20360 ATTN: Code 6101	1
Army Research Office P.O. Box 12211 Triangle Park, NC 27709 ATTN: Metallurgy & Ceramics Program	1
Army Materials and Mechanics Research Center Watertown, MA 02172 ATTN: Research Programs Office	1
Air Force Office of Scientific Research Bldg. 410 Bolling Air Force Base Washington, DC 20332 ATTN: Chemical Science Directorate	1
Electronics & Solid State Sciences Directorate	1
Air Force Materials Laboratory Wright-Patterson AFB Dayton, OH 45433	1
Library Building 50, Rm 134 Lawrence Radiation Laboratory Berkeley, CA	1

Organization	Copies
NASA Headquarters Washington, DC 20546 ATTN: Code RRM	1
NASA Lewis Research Center 21000 Brookpark Road Cleveland, OH 44135 ATTN: Library	1
National Bureau of Standards Washington, DC 20234 ATTN: Metallurgy Division	1
Inorganic Materials Div.	1
Director Applied Physics Laboratory University of Washington 1013 Northeast Forthieth Street Seattle, WA 98105	1
Defense Metals and Ceramics Information Center Battelle Memorial Institute 505 King Avenue Columbus, OH 43201	1
Metals and Ceramics Division Oak Ridge National Laboratory P.O. Box X Oak Ridge, TN 37380	1
Los Alamos Scientific Laboratory P.O. Box 1663 Los Alamos, NM 87544 ATTN: Report Librarian	1
Argonne National Laboratory Metallurgy Division P.O. Box 229 Lemont, IL 60439	1
Brookhaven National Laboratory Technical Information Division Upton, Long Island New York 11973 ATTN: Research Library	1
Office of Naval Research Branch Office 1030 East Green Street Pasadena, CA 91106	1

C
April 1978

SUPPLEMENTARY DISTRIBUTION LIST

Technical and Summary Reports

Dr. T. R. Beck
Electrochemical Technology Corporation
10035 31st Avenue, NE
Seattle, Washington 98125

Professor I. M. Bernstein
Carnegie-Mellon University
Schenley Park
Pittsburgh, Pennsylvania 15213

Professor H. K. Birnbaum
University of Illinois
Department of Metallurgy
Urbana, Illinois 61801

Dr. Otto Buck
Rockwell International
1049 Camino Dos Rios
P. O. Box 1085
Thousand Oaks, California 91360

Dr. David L. Davidson
Southwest Research Institute
8500 Culebra Road
P. O. Drawer 28510
San Antonio, Texas 78284

Dr. D. J. Duquette
Department of Metallurgical Engineering
Rensselaer Polytechnic Institute
Troy, New York 12181

Professor R. T. Foley
The American University
Department of Chemistry
Washington, D. C. 20016

Mr. G. A. Gehring
Ocean City Research Corporation
Tennessee Avenue & Beach Thorofare
Ocean City, New Jersey 08226

Dr. J. A. S. Green
Martin Marietta Corporation
1450 South Rolling Road
Baltimore, Maryland 21227

Professor R. H. Heidersbach
University of Rhode Island
Department of Ocean Engineering
Kingston, Rhode Island 02881

Professor H. Herman
State University of New York
Material Sciences Division
Stony Brook, New York 11794

Professor J. P. Hirth
Ohio State University
Metallurgical Engineering
Columbus, Ohio 43210

Dr. E. W. Johnson
Westinghouse Electric Corporation
Research and Development Center
1310 Beulah Road
Pittsburgh, Pennsylvania 15235

Professor R. M. Latanision
Massachusetts Institute of Technology
77 Massachusetts Avenue
Room 8-202
Cambridge, Massachusetts 02139

Dr. F. Mansfeld
Rockwell International Science Center
1049 Camino Dos Rios
P. O. Box 1085
Thousand Oaks, California 91360

Professor H. W. Pickering
Pennsylvania State University
Department of Material Sciences
University Park, Pennsylvania 16802

Dr. E. A. Starke, Jr.
Georgia Institute of Technology
School of Chemical Engineering
Atlanta, Georgia 30332

Dr. Barry C. Syrett
Stanford Research Institute
333 Ravenswood Avenue
Menlo Park, California 94025

C
April 1978

SUPPLEMENTARY DISTRIBUTION LIST
(Continued)

Dr. R. P. Wei
Lehigh University
Institute for Fracture and
Solid Mechanics
Bethlehem, Pennsylvania 18015

Professor H. G. F. Wilsdorf
University of Virginia
Department of Materials Science
Charlottesville, Virginia 22903

Prof. J. B. Cohen
Dept. of Materials Science & Engineering
The Technological Institute
Northwestern University
Evanston, Illinois 60201

Prof. H. W. Liu
Dept. of Chemical Engineering & Materials Science
L. C. Smith College of Engineering
Syracuse University
Syracuse, NY 13210

Dr. S. P. Rideout
Savannah River Laboratory
E. I. duPont de Nemours & Co.
Aiken, South Carolina 29801

Prof. R. W. Staehle
Dept. of Metallurgical Engineering
The Ohio State University
Columbus, Ohio 43210